



HAL
open science

Quantum dynamics of the charge transfer in $C^+ + S$ at low collision energies

Aurélie Chenel, Etienne Manguad, Yves Justum, Dahbia Talbi,
Marie-Christine Bacchus-Montabonel, Michèle Desouter-Lecomte

► **To cite this version:**

Aurélie Chenel, Etienne Manguad, Yves Justum, Dahbia Talbi, Marie-Christine Bacchus-Montabonel, et al.. Quantum dynamics of the charge transfer in $C^+ + S$ at low collision energies. *Journal of Physics B: Atomic, Molecular and Optical Physics*, 2010, 43 (24), pp.245701. 10.1088/0953-4075/43/24/245701 . hal-00580352

HAL Id: hal-00580352

<https://hal.science/hal-00580352>

Submitted on 28 Mar 2011

HAL is a multi-disciplinary open access archive for the deposit and dissemination of scientific research documents, whether they are published or not. The documents may come from teaching and research institutions in France or abroad, or from public or private research centers.

L'archive ouverte pluridisciplinaire **HAL**, est destinée au dépôt et à la diffusion de documents scientifiques de niveau recherche, publiés ou non, émanant des établissements d'enseignement et de recherche français ou étrangers, des laboratoires publics ou privés.

Quantum dynamics of the charge-transfer in $C^+ + S$ at low collision energies

Aurélie Chenel¹, Etienne Mangaud¹, Yves Justum¹, Dahbia Talbi², Marie-Christine Bacchus-Montabonel³ and Michèle Desouter-Lecomte^{1,4}

¹ Laboratoire de Chimie Physique, Bât 349, Univ-ParisSud et CNRS-UMR8000, F-91405 Orsay Cedex, France.

² Groupe de Recherche en Astronomie et Astrophysique du Languedoc, Université de Montpellier II et CNRS-UMR5024, Place Eugène Bataillon, F-34095 Montpellier Cedex 05, France

³ Laboratoire de Spectrométrie Ionique et moléculaire, Université de Lyon I et CNRS-UMR5579, 43 Bd du 11 Novembre 1918, F-69622 Villeurbanne Cedex, France

⁴ Département de Chimie, B6c, Université de Liège, Sart-Tilman, B-4000, Liège 1, Belgium.

E-mail : michele.desouter-lecomte@u-psud.fr

Abstract

Following a recent semiclassical investigation by Bacchus-Montabonel M C and Talbi D (2008 *Chem. Phys. Lett.* **467**, 28), the $C^+(2s^22p)^2P + S(3s^23p^4)^3P$ charge transfer process involved in the modellisation of the interstellar medium chemistry and its reverse reaction are revisited by combining a wave packet approach and semiclassical dynamics in a quasimolecular approach for doublet and quartet states. New radial non adiabatic coupling matrix elements have been calculated and the mixed treatment gives access to new precise values of the rate coefficients for the direct and reverse charge transfer processes. For this system, quantum and semiclassical results are in good agreement even at low collision kinetic energies. The dominance of the quartet states in the process is confirmed. In the quantum treatment, the collision matrix elements are extracted from wave packets by the flux method with an absorbing potential. The formation of resonances due to a centrifugal barrier is illustrated.

1. Introduction

A quantitative analysis of the emission-line spectra of ionized astronomical objects requires reliable data on the microscopic ionization and recombination processes involved. Recombination may occur either by radiative or dielectronic capture or by charge transfer from neutral species. The charge transfer recombination process with atomic and molecular hydrogen or atomic helium is particularly important in astrophysical plasmas for many multiply-charged ions, whose emission lines are used to provide direct information of the ionization structure of astronomical objects [1,2,3,4,5,6,7,8]. Such processes have anyway to be enlarged in order to describe the formation of more complex molecules. In that sense, the charge transfer $C^+ + S$ has been shown to be one of the key reactions for the chemistry of sulphur and carbon species in the interstellar medium. Indeed, this reaction plays an important role in the formation and abundance of H_2CS in the dense interstellar clouds. It is a crucial process for the chemistry of photon dominated regions (PDR's) [9,10] since it allows the enhancement of the ionic carbon chemistry at the origin of the formation of the complex carbon molecules observed in the PDR's.

In astrochemical models, the rate constant of the $C^+ + S$ charge transfer is generally estimated by a single value of $1.5 \times 10^{-9} \text{ cm}^3 \text{ s}^{-1}$ [11] for the 10K- 41000K temperature range. This value is uncertain for such a large temperature domain and detailed calculations had to be performed. In a previous paper [12], an *ab initio* molecular treatment of the direct $C^+(2s^2 2p)^2P + S(3s^2 3p^4)^3P$ process and its reverse $C + S^+$ reaction has been carried out by using a semi-classical dynamical method. Such an approach, largely used in the 100eV-keV energy range may be however questionable in the low eV energy range. The direct charge transfer has thus been revisited using a quantum wave packet propagation method and a comparison of both approaches has been developed. An evaluation of the rate coefficients for the reverse process $C(2s^2 2p^2)^3P + S^+(3s^2 3p^3)^4P$ has also been deduced using the symmetry properties of the collision matrix.

2. Theoretical treatment

2. 1. Molecular Hamiltonian

The Hamiltonian of the CS^+ molecular ion is the sum of the radial and rotational parts of the kinetic energy and the electronic Hamiltonian

$$H = T_R + T_{rot} + H^{el}.$$

The spin-orbit effects are neglected in this work so doublet and quartet manifolds are considered separately. The spin is decoupled and taken into account only via its multiplicity when calculating the charge transfer cross section. The total time dependent wave function is expanded in a parity adapted ro-electronic basis set which therefore corresponds to the expression for singlet states [13, 14]

$$\zeta_{mKM\Omega} = \frac{1}{[2(1+\delta_{\Lambda 0})]^{1/2}} [\psi_{m\Lambda} | KM\Omega\rangle + (-1)^K \varepsilon \psi_{m,-\Lambda} | KM, -\Omega\rangle] \quad (1-1)$$

where m numbers the electronic states $\psi_{m\Lambda}$ and Λ is the quantum number for the projection on the molecular axis of the total electronic orbital angular momentum \mathbf{L} . We consider here Σ ($\Lambda = 0$) and Π ($\Lambda = 1$) states. The total angular momentum is here $\mathbf{K} = \mathbf{N} + \mathbf{L}$ where \mathbf{N} is the rotational angular momentum. $|KM\Omega\rangle$ are the states of the total angular momentum representation of quantum number K . M and Ω are the projection of the total angular momentum on the laboratory Z axis and on the internuclear z axis respectively [13]. The two cases $\varepsilon = 1$ and $\varepsilon = -1$ correspond to e and f states.

The adiabatic electronic functions $\psi_{m\Lambda}^{adia}$ diagonalize H^{el} . The charge transfer process is driven mainly by non-adiabatic interactions in the vicinity of avoided crossings [15]. The corresponding radial coupling matrix elements between all pairs of states of the same symmetry and multiplicity were calculated by means of the finite difference technique:

$$F_{m\Lambda, n\Lambda}(R) = \langle \psi_{m\Lambda}^{adia} | \partial_R | \psi_{n\Lambda}^{adia} \rangle = \lim_{\Delta \rightarrow 0} \frac{1}{\Delta} \langle \psi_{m\Lambda}^{adia}(R) | \psi_{n\Lambda}^{adia}(R + \Delta) \rangle, \quad (1-2)$$

with the parameter $\Delta = 0.0012$ a.u. previously tested [16]. For reasons of numerical accuracy, we performed a three-point numerical differentiation using calculations at $R + \Delta$ and $R - \Delta$ for a very large number of interatomic distances in the avoided-crossing region. In a diatomic system, this \mathbf{F} matrix enables us to build diabatic states $\psi_{K\Lambda}^{dia}$ which rigorously remove all the interactions due to T_R and are coupled by smooth potential elements of H^{el} [17]. The adiabatic-to-diabatic transformation matrix $\mathbf{D}(R)$ is obtained by solving the equation $\partial_R \mathbf{D}(R) + \mathbf{F} \cdot \mathbf{D}(R) = 0$ with the asymptotic condition $\mathbf{D}(R_\infty) = \mathbf{I}$ where \mathbf{I} is the identity matrix.

The rotational part of the kinetic energy is written by neglecting all the spin-orbit or spin-rotation couplings. As in a pure b Hund case, the spin projection Σ on the intermolecular axis is zero and $\Omega = \Lambda + \Sigma = \Lambda$. With these assumptions T_{rot} reads: [13]

$$T_{rot} = N^2 B = (K^2 + L^2 - 2K_z L_z - K_+ L_- - K_- L_+) B \quad (1-3)$$

where $B = \hbar^2 / 2\mu R^2$ and μ is the reduced mass. By applying the usual expressions of the ladder operators for L_{\pm} and the unusual ones for K_{\pm} ($K_{\pm} |K\Lambda M\rangle = [K(K+1) - \Lambda(\Lambda \mp 1)]^{1/2} |K, \Lambda \mp 1, M\rangle$ [18]), the matrix elements in the ro-electronic basis set can be related to the matrix elements $\langle m\Sigma | iL_y | nB_1 \rangle = a_{mn}$ and $\langle m\Sigma | iL_x | nB_2 \rangle = -a_{mn}$ with $|n\Lambda = \pm 1\rangle = \frac{1}{\sqrt{2}} (\pm |nB_1\rangle + i |nB_2\rangle)$ computed by the MOLPRO software [19]. One finally gets from Eq.(1-3) by neglecting the contribution from $L_x^2 + L_y^2$:

$$T_{rot}^{dia} = [K(K+1) - \Lambda^2] B \delta_{mm'} \delta_{\Lambda\Lambda'} \delta_{K,K'} \delta_{MM'} + \sqrt{K(K+1)} 2a_{mm'} B \delta_{\Sigma\Pi} \delta_{K,K'} \delta_{MM'}$$

The matrix is transformed to the diabatic representation by the $\mathbf{D}(R)$ matrix. The total angular momentum and its projection on the Z axis being conserved, the coupled equations for the radial part of the nuclear functions are decoupled according to K and M . We consider the $M = 0$ manifold and this quantum number will be omitted throughout. For each value of K , the coupled equations for the radial functions $\chi_{m\Lambda}^{dia,K}(R, t)$ corresponding to the electronic channels in the diabatic representation take the form

$$\chi^{dia,K}(R, t) = e^{\frac{-i\mathbf{H}^{dia,K}(t-t_0)}{\hbar}} \chi^{dia,K}(R, t_0) \quad (1-4)$$

where

$$\mathbf{H}^{dia,K}(R) = \hbar^2 \left(-\frac{1}{2\mu} \frac{\partial^2}{\partial R^2} + \frac{K(K+1) - \Lambda^2}{2\mu R^2} \right) \times \mathbf{I} + \mathbf{H}^{el,dia}(R) + \mathbf{T}_{rot}^{dia,K}(R) \quad (1-5)$$

$\mathbf{T}_{rot}^{dia,K}(R)$ contains the rotational off diagonal elements in the diabatic representation.

In the semi-classical collision treatment, the rotational coupling matrix elements $\langle \psi_{m\Lambda} | iL_y | \psi_{n\Lambda'} \rangle$ between Σ - Π molecular states are determined directly from the quadrupole moment tensor using also the MOLPRO software [19]. This allows the determination of translation effects knowing the quadrupole moment tensor [20]. In the approximation of the

common translation factor [21], the radial and rotational coupling matrix elements between states $\psi_{m\Lambda}^{adia}$ and $\psi_{n\Lambda'}^{adia}$ may indeed be transformed respectively into

$$\langle \psi_{m\Lambda}^{adia} | \partial_R - (\epsilon_{m\Lambda} - \epsilon_{n\Lambda'}) z^2 / 2R | \psi_{n\Lambda'}^{adia} \rangle \text{ and } \langle \psi_{m\Lambda}^{adia} | iL_y + (\epsilon_{m\Lambda} - \epsilon_{n\Lambda'}) z x | \psi_{n\Lambda'}^{adia} \rangle,$$

where $\epsilon_{m\Lambda}$ and $\epsilon_{n\Lambda'}$ are the electronic energies of states $\psi_{m\Lambda}^{adia}$ and $\psi_{n\Lambda'}^{adia}$ and z^2 and zx are the component of the quadrupole moment tensor.

2. 2. Collision dynamics

In the quantum approach, the square modulus of the collision matrix elements $|S_{n\Lambda',m\Lambda}^K(E)|^2$ are computed from the flux operator in the asymptotic region where the diffusion eigenstates take the form

$$|\Psi_{m\Lambda}^{+,K}(E)\rangle \xrightarrow{R \rightarrow \infty} |\Phi_{m\Lambda}^{-,K}(E)\rangle - \sum_{n,\Lambda'} S_{n\Lambda',m\Lambda}^K(E) |\Phi_{n\Lambda'}^{+,K}(E)\rangle$$

where $|\Phi_{m\Lambda}^{\pm,K}(E)\rangle = \sqrt{\frac{\mu}{2\pi\hbar k_{m\Lambda}}} h_K^{\pm}(k_{m\Lambda}R) \zeta_{m\Lambda K}$. $k_{m\Lambda}$ is the wave number in the ro-electronic

channel $m\Lambda K$ and $h_K^{\pm}(k_{m\Lambda}R)$ is the Hankel-Riccati function imposed by the long range

$K(K+1)/R^2$ potential [22]. The elements $|S_{n\Lambda',m\Lambda}^K(E)|^2$ are related to the average value of the

flux operator $F = \frac{-i\hbar}{2\mu} (\partial_R \delta(R - R_{as}) + \delta(R - R_{as}) \partial_R)$ at an asymptotic coordinate R_{as}

computed with the radial parts in an exit channel $\bar{\chi}_{n\Lambda'}^K(R, E) = \langle \zeta_{n\Lambda' K} | \Psi_{m\Lambda}^{+,K}(E) \rangle$ where integration is over electronic coordinates and angles. One has:

$$\langle \bar{\chi}_{n\Lambda'}^K(R, E) | F | \bar{\chi}_{n\Lambda'}^K(R, E) \rangle = \frac{1}{2\pi} |S_{n\Lambda',m\Lambda}^K(E)|^2 \quad (2-1)$$

These radial parts for all the electronic exit channels and a given K are represented by a vector

$\bar{\chi}^K(R, E)$. They are obtained by Fourier transforming the components of a radial wave packet

when it comes back in the asymptotic region after the collision. The initial radial wave packet

$\chi^K(R, t=0)$ has a Gaussian component in the entrance channel $\zeta_{m\Lambda K}$ with no outgoing

momentum $\chi_{m\Lambda}^K(R, t=0) = g(R)$, with

$$g(R) = \frac{1}{\sqrt{\sigma\sqrt{2/\pi}}} \exp \left[ik_{m\Lambda} R - \frac{(R - R_0)^2}{\sigma^2} \right] \quad (2-2)$$

and zero component in all other channels. One then has

$$\bar{\chi}^K(R, E) = \frac{1}{2\pi c(K, E)} \int_{-\infty}^{\infty} e^{iEt/\hbar} e^{-i\mathbf{H}^{dia,K}t/\hbar} \chi^K(R, t=0) dt \quad (2-3)$$

where the $\mathbf{H}^{dia,K}$ matrix has been defined in Eq. (1-5) and $c(K, E)$ is the amplitude of the stationary states in the initial wave packet

$$c(K, E) = \langle \Psi_{m\Lambda}^{+,K}(E) | g(R) \zeta_{m\Lambda K} \rangle = \sqrt{\frac{\mu}{2\pi\hbar k_{m\Lambda}}} \int_0^{\infty} h_K^-(k_{m\Lambda} R)^* g(R) dR. \quad (2-4)$$

The average of the flux operator is then computed by using the properties of a complex absorbing potential (CAP) in the asymptotic region as suggested by Jäckle and Meyer [23] and already implemented in different systems [24, 25]. The flux operator is expressed as

$F = \frac{i}{\hbar} [H, \Theta]$ where $\Theta(R) = 0$ for $R < R_{as}$ and $\Theta(R) = 1$ for $R > R_{as}$. The Hamiltonian is modified by adding a complex absorbing potential $H \rightarrow H - iW$ where $W(R) = \eta(R - R_{as})^2$.

The final expression for $|S_{n\Lambda', m\Lambda}^K(E)|^2$ is then the average of the absorbing potential computed with the functions (2-3)

$$|S_{n\Lambda', m\Lambda}^K(E)|^2 = 2 \langle \bar{\chi}_{n\Lambda'}^K(R, E) | W | \bar{\chi}_{n\Lambda'}^K(R, E) \rangle. \quad (2-5)$$

The procedure can be summarized as follows: a Gaussian wave packet in entrance channel $\zeta_{m\Lambda K}$ is propagated by the coupled equations in the diabatic representation by using the split operator formalism [26] extended to take into account non adiabatic interactions [27]. On exit, when the norm begins to decrease due to the CAP, the functions $\chi_{n\Lambda'}^K(R, t)$ are recorded in the range $R > R_{as}$. The propagation is stopped when the norm is smaller than a threshold fixed to 10^{-6} ensuring that all the wave packet has been absorbed. The $\chi_{n\Lambda'}^K(R, t)$ for $R > R_{as}$ are Fourier transformed to get the eigenstates $\bar{\chi}_{n\Lambda'}^K(R, E)$ in the same domain by using the amplitude $c(K, E)$ [Eq. (2-3)] and finally $|S_{n\Lambda', m\Lambda}^K(E)|^2$ is given by Eq. (2-5).

The cross section for the transfer of an electron from an initial state $\psi_{m\Lambda}$ to a final state $\psi_{n\Lambda'}$ is obtained by summing over the total angular momentum values up to convergence

$$\sigma_{n\Lambda', m\Lambda}(E) = \frac{\pi}{k_{m\Lambda}^2(E)} \sum_K (2K+1) |S_{n\Lambda', m\Lambda}^K(E) - \delta_{nm} \delta_{\Lambda'\Lambda}|^2 \quad (2-6)$$

Note that the propagations for different K are independent so that this summation can be expanded in parallel on several processors.

In the semiclassical approach, the nuclei are considered to follow a classical trajectory $R(t) = b + vt$ with regard to the impact parameter b and the velocity v [28]. The time-Schrödinger equation reduces thus to:

$$\left(H^{el} [r, R(t)] - i \frac{\partial}{\partial t} \right) \times \Psi(r, b, v, t) = 0 \quad (2-7)$$

where r are for the electronic coordinates. It may be solved for each velocity v and impact parameter b by expanding the total wave function on the eigenfunctions $\psi_{m\Lambda}^{adia}$ of H^{el} with eigenvalues $\epsilon_{m\Lambda}$:

$$\Psi(r, b, v, t) = \sum_{m\Lambda} a_{m\Lambda}(b, v, t) \psi_{m\Lambda}^{adia} [r, R(t)] \times \exp \left(-i \int_0^t \epsilon_{m\Lambda} [R(t')] dt' \right).$$

By integration of equation (2-7), the capture probabilities are given by $P(b, v) = \sum_{m\Lambda} |a_{m\Lambda}(b, v, \infty)|^2$ with summation over all charge exchange channels. The cross section is then defined by:

$$\sigma(v) = \frac{1}{4\pi} \int P(b, v) db \quad (2-8)$$

The collision dynamics was treated from keV to eV energies by a semi-classical approach using the EIKONXS program [29]. Both radial and rotational coupling matrix elements were taken into account, as well as translation effects, although they are expected to be low at these energies.

2. 3. Thermal rate constant

The rate constants $k(T)$ were calculated by averaging the cross sections $\sigma(E)$ over a Maxwellian velocity distribution at temperature T :

$$k(T) = \left(\frac{8}{\pi\mu} \right)^{1/2} \left(\frac{1}{k_B T} \right)^{3/2} \int_0^\infty E \sigma(E) \times \exp \left(-\frac{E}{k_B T} \right) dE \quad (2-9)$$

The rate constant for the reverse ionization process $k_{rev}(T)$ may be determined easily by means of the micro reversibility relation from the corresponding charge transfer rate constant $k(T)$:

$$k_{rev}(T) = g \exp\left(-\frac{\Delta E}{k_B T}\right) k(T), \quad (2-8)$$

where g is the ratio of the statistical weights of initial and final states, and ΔE is the energy gain of the charge transfer reaction.

3. Charge transfer in the CS^+ system

3. 1. Adiabatic states and couplings

The adiabatic potential energy curves have been calculated using the MOLPRO suite of *ab-initio* programs [19] at the state average CASSCF-MRCI level of theory. The active space includes the $n = 2$ orbitals for carbon and $n = 3$ orbitals for sulphur. The ECP10sdf relativistic pseudo-potential has been used to describe the 10 core-electrons of sulphur [30] with the correlation-consistent aug-cc-pVQZ basis sets of Dunning [31] for all atoms. The molecular treatment has been revisited with a very detailed analysis in order to avoid artefacts for the determination of the radial coupling matrix elements. In that sense, the calculation has been performed for a very great number of internuclear distances in order to assure the continuity between the successive geometries and provide the maximum precision for the determination of the radial coupling matrix elements which are therefore more accurate than the previous values given in ref.12.

The process occurring at low temperatures, the different species are supposed to be present in their ground state. With regard to the correlation diagram [12], only two molecular states $\{C^+(2s^2 2p)^2P + S(3s^2 3p^4)^3P\}$ and $\{C(2s^2 2p^2)^3P + S^+(3s^2 3p^3)^4S\}$ corresponding to the ground atomic levels would be involved in the charge transfer reaction. Table I displays the lowest levels of the correlation diagram:

Table I : Correlation diagram

Configuration	Molecular states	Asymptotic energy (eV) [32]
---------------	------------------	-----------------------------

$C(2s^22p^2)^1D + S^+(3s^23p^3)^4S$	$^4\Sigma, ^4\Pi, ^4\Delta$	1.26
$C^+(2s^22p)^2P + S(3s^23p^4)^3P$	$^{2,4}\Sigma, ^{2,4}\Pi, ^{2,4}\Delta$	0.92
$C(2s^22p^2)^3P + S^+(3s^23p^3)^4S$	$^{2,4,6}\Sigma, ^{2,4,6}\Pi$	0.0

Effectively, two states only are involved in the doublet manifold presented in Fig.1a and no significant interaction occurs with higher levels. The $^2\Sigma$ and $^2\Pi$ potentials show a smooth avoided crossing around $R = 5$ a.u., in agreement with the previous calculations of Larsson [33] and Honjou [34]. The corresponding radial coupling matrix elements displayed in Fig. 2a are, respectively, 0.823 a.u. and 0.459 a.u. high for $^2\Sigma$ and $^2\Pi$ states. A detailed calculation at short range exhibits besides a sharp radial coupling peak, 6.475 a.u. high, at $R = 1.8$ a.u. in the repulsive part of the potential energy curves between the $^2\Pi$ states. Such interaction has, of course, to be taken into account but would probably appear as quasi-diabatic in the collision dynamics.

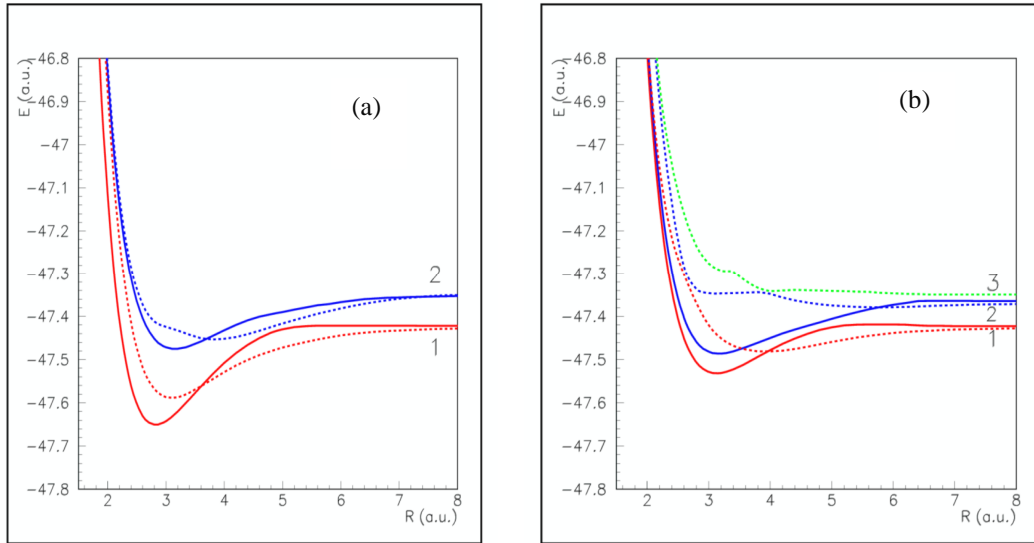


Fig. 1: Adiabatic potential energy curves for the Σ (full lines) and Π (dashed lines) states of the CS^+ molecular system. **(a)** doublet manifold; **(b)** quartet manifold.

1. $\{ C(2s^22p^2)^3P + S^+(3s^23p^3)^4S \}$
2. $\{ C^+(2s^22p)^2P + S(3s^23p^4)^3P \}$ entry channel
3. $\{ C(2s^22p^2)^1D + S^+(3s^23p^3)^4S \}$

For the quartet manifold, a similar smooth avoided crossing is observed for the $^4\Sigma$ potential energy curves around $R = 5$ a.u.. However, for the $^4\Pi$ states, a strong interaction

with the higher ${}^4\Pi\{C(2s^22p^2)^1D + S^+(3s^23p^3)^4S\}$ channel corresponding to the excited 1D state of the carbon atom occurs around $R = 4$ a.u. as shown on Fig. 1b, and three ${}^4\Pi$ states have to be considered in the calculation. Such interaction is not observed between the ${}^4\Sigma$ levels and only the two lowest ${}^4\Sigma$ levels are involved in the charge transfer process. The corresponding radial coupling matrix elements are presented in Fig. 2b. A smooth peak, 0.915 a.u. high is observed for the radial coupling between the ${}^4\Sigma$ states, relatively similar to the interaction between ${}^2\Sigma$ levels. However, the radial coupling between the entry channel and the ${}^4\Pi\{C(2s^22p^2)^1D + S^+(3s^23p^3)^4S\}$ state reaches up to 10.093 a.u. in absolute value at $R = 3.87$ a.u. and may be determinant in the collision dynamics. An extremely sharp radial coupling matrix element between the two lowest ${}^4\Pi$ levels is also exhibited at short range. Such interaction in the repulsive part of the potential energy curve would certainly be considered as quasi-diabatic in the collision dynamics. The ${}^{2,4}\Delta$ states correlated by means of rotational coupling have not been considered in the calculation as the corresponding entry channel could be correlated only to excited states. The ${}^6\Sigma, {}^6\Pi\{C(2s^22p^2)^3P + S^+(3s^23p^3)^4S\}$ levels cannot be involved in the process for spin symmetry reasons.

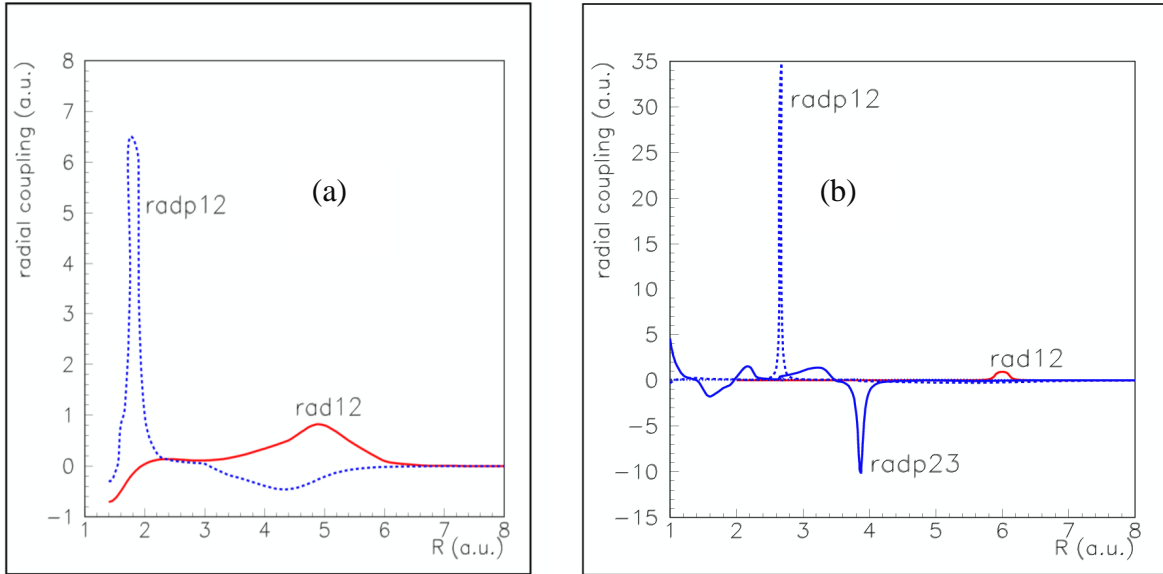


Fig. 2: Radial coupling matrix elements between Σ (rad12, red lines) and Π (radp12, radp23, blue lines) states of the CS^+ molecular system. **(a)** doublet manifold; **(b)** quartet manifold (same labels as in Fig. 1)

3. 2. Cross section by wave packet dynamics

Numerous parameters must be controlled to ensure convergence of the cross section. The main point is that the whole wave packet be smoothly and totally absorbed in the CAP

after the collision. The spreading of the Gaussian wave packet in the entrance channel and a very low average kinetic energy are two unfavourable factors. In principle a thin Gaussian wave packet would contain information on a broad range of energy. However such wave packets are difficult to treat numerically due to their early spreading. It appears more convenient to use large wave packet with a width of about $\sigma \approx 1.5$ a.u. [Eq.(2-2)]. The spreading is then slow and the wave packet remains more compact even after the collision. The length of the grid is fixed by verifying that the populations in the different electronic states reach a constant value before entering the CAP. Some rotational couplings are not peaked as radial couplings and they induce small Rabi oscillations which damp very slowly enforcing long grids. The initial position R_0 of the wave packet and the abscissa R_{as} of the CAP are shifted towards large R with increasing K (for a relative kinetic energy of 1 eV, convergence is reached for $K \approx 300$ and for 10eV around $K \approx 900$). We have used grid up to 200 bohr. For each collision energy and grid length, the number of grid points is determined by $dR < \pi/k_{max}$ where k_{max} is the largest wave number. We check that $\sum_{n\Lambda'} |S_{n\Lambda',m\Lambda}^K(E)|^2 = 1$ for each K with a tolerance of 0.01%. The propagation duration is automatically determined by the criterion that the norm becomes smaller than 10^{-6} .

Another crucial situation is the formation of quasi bound states with long lifetimes which prevent the norm from decaying below this threshold. Fig. 3 gives the probability to be in the exit channel $1^4\Sigma \{C(2s^22p^2)^3P + S^+(3s^23p^3)^4S\}$ when the entrance channel is $2^4\Sigma \{C^+(2s^22p)^2P + S(3s^23p^4)^3P\}$ for different values of the total angular momentum K . One observes the constant asymptotic values excepted for some K (for instance $K = 220$) when shape resonances due to a barrier in the effective potential are populated. Then the population oscillates because some components remain in the bound part of the effective potential for a long time and too long computational times should be necessary to satisfy the criterion of a norm smaller than 10^{-6} .

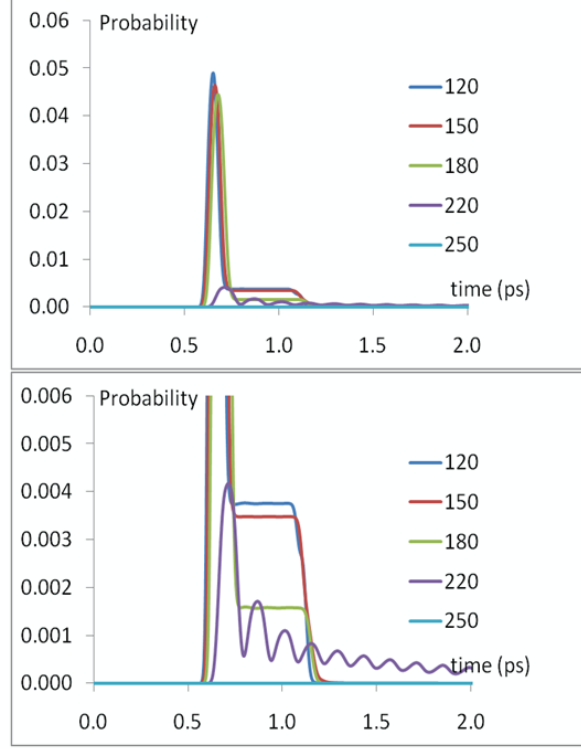


Fig. 3. Probability of occupying the exit channel $1^4\Sigma\{C(2s^22p^2)^3P + S^+(3s^23p^3)^4S\}$ when the entrance channel is $2^4\Sigma\{C^+(2s^22p)^2P + S(3s^23p^4)^3P\}$ for a mean kinetic energy $E_{CM} = 1\text{ eV}$ and different values of the total angular momentum K . Lower panel: zoom on the low probabilities

The process is illustrated in Figs. 4 and 5. The effective potential of the entry channel $2^4\Sigma\{C^+(2s^22p)^2P + S(3s^23p^4)^3P\}$ and exit channel $1^4\Sigma\{C(2s^22p^2)^3P + S^+(3s^23p^3)^4S\}$ for $K = 220$ are drawn in Fig. 4. The mean kinetic energy is $E_{CM} = 1\text{ eV}$ and is represented by a dashed line. The arrow shows the region of non-adiabatic radial coupling (see Fig. 2). One sees that shape resonance can be formed in the entry channel since for this energy the well behind the barrier due to the centrifugal term can be reached by tunnelling. The metastable states occur roughly at the energies of bound states in the corresponding uncoupled well. The precise determination of the resonances is not the subject of this work and time dependent methods are not appropriate because too long propagation times should be necessary. However, we have observed the process and verify that the contribution to the cross section is negligible in this case. In this example the trapped population in the metastable state in the entrance channel will interact with the exit channel $1^4\Sigma$ by the non adiabatic radial coupling around $R = 6\text{ a.u.}$. This component remains trapped again in the well in the effective potential of $1^4\Sigma$. This behaviour is illustrated in Fig.5.

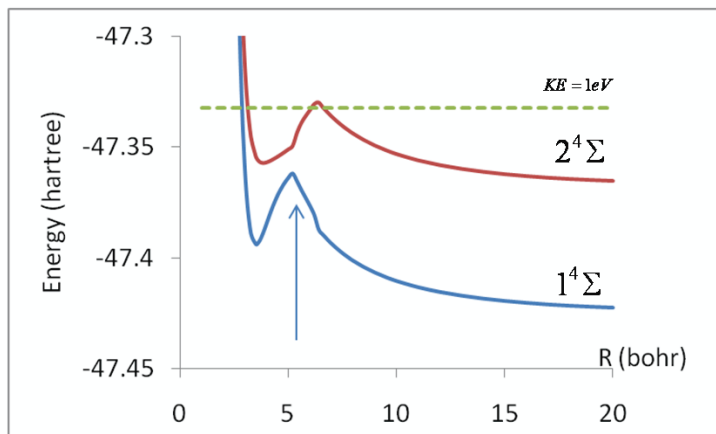


Fig. 4. Effective potential for the entrance channel $2^4\Sigma$ $\{C^+(2s^22p)^2P + S(3s^23p^4)^3P\}$ and the exit channel $1^4\Sigma$ $\{C(2s^22p)^3P + S^+(3s^23p^3)^4S\}$ for a mean relative kinetic energy of $E_{CM} = 1\text{eV}$ (dashed line $KE = 1\text{eV}$) and a total angular momentum $K = 220$. The arrow indicates the location of the radial non adiabatic coupling.

Fig. 5 shows the components of the wave packet for $K = 220$ in the entrance $2^4\Sigma$ (upper panels) and $1^4\Sigma$ (lower panels) channels for two times during the collision. The initial position is $R_0 = 60$ a.u. [Eq. (2-2)]. One observes the trapped populations in both channels. However, this quasibound component is very small and should contribute very few to the cross section. At this collision energy, the most populated channel is the $2^4\Pi$ state which is not a charge transfer channel. When metastable states are formed in an exit channel, the test of a final norm smaller than 10^{-6} to stop the propagation becomes inefficient and a careful analysis is necessary.

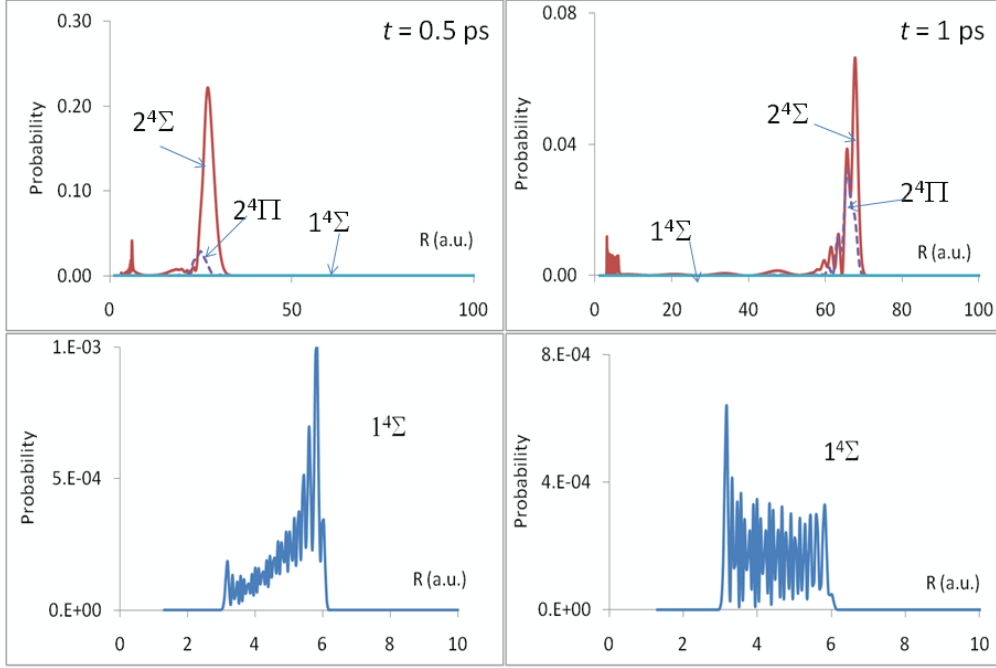


Fig. 5. Components of the wave packets during the collision for a mean relative kinetic energy of $E_{\text{CM}} = 1\text{eV}$ and $K = 220$ in the quartet manifold. Upper panels: population in the entrance channel $2^4\Sigma$ $\{ C^+(2s^22p)^2P + S(3s^23p^4)^3P \}$ (full line) and in the most populated exit channel $2^4\Pi$ (dashed line) which is not a charge exchange channel; lower panels: zoom on the population in the exit channel $1^4\Sigma$ $\{ C(2s^22p^2)^3P + S^+(3s^23p^3)^4S \}$ leading to the formation of metastable states. The initial wave packet is a Gaussian [Eq. (2-2)] centered at $R_0 = 60$ bohr. The initial width is $\sigma = 1.5$ bohr.

Some examples of computations are given for the doublet manifold in Figs. 6 and 7. Partial cross sections towards exit electronic channels $2^2\Sigma \rightarrow 1^2\Sigma$ and $2^2\Sigma \rightarrow 1^2\Pi$ as a function of K are drawn in Fig. 6a and 6b respectively. The relative energy E_{CM} is 2 eV. Convergence of the summation in Eq. (2-6) is reached around $K = 320$ in this case. The cross section of the process driven by radial coupling $2^2\Sigma \rightarrow 1^2\Sigma$ exceeds that due to rotational coupling $2^2\Sigma \rightarrow 1^2\Pi$ by two orders of magnitude. However the radial coupling is not always the main factor for charge exchange as shown in Fig. 7.

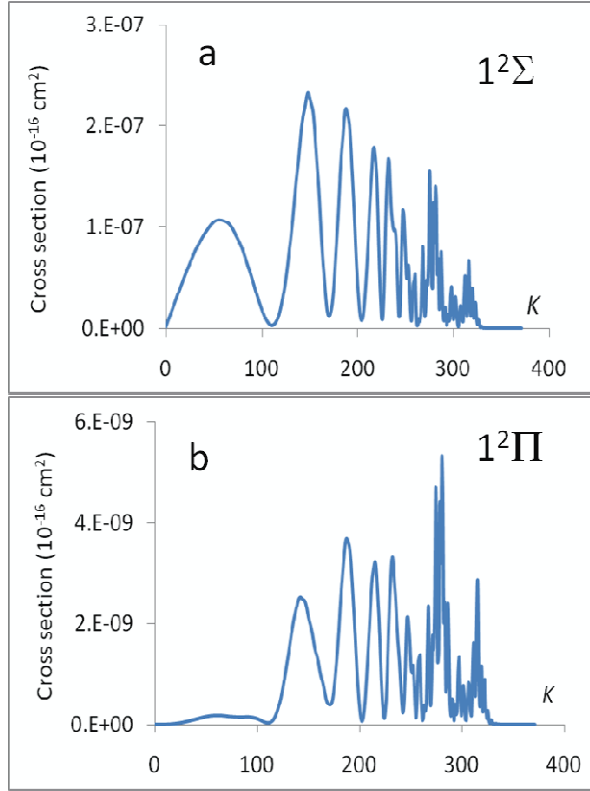


Fig. 6. Partial cross section as a function of the total angular momentum K for a relative energy $E_{\text{CM}} = 2\text{eV}$. The entrance channel is $2^2\Sigma \{C(2s^22p^2)^3P + S^+(3s^23p^3)^2D\}$. Panel (a): exit channel $1^2\Sigma \{C^+(2s^22p)^2P + S(3s^23p^4)^1D\}$ (radial coupling), panel (b) $1^2\Pi \{C^+(2s^22p)^2P + S(3s^23p^4)^1D\}$ (rotational coupling).

The cross sections for each exit channel computed by Eq. (2-6) are given in Fig. 7 for two entry channels in the range 0.5 to 10 eV. One observes that the cross sections involving radial couplings have a relative value in agreement with the strength of the interaction (see Fig. 2). For instance, there is a factor 10^2 between the cross sections for $2^2\Sigma \rightarrow 1^2\Sigma$ (Fig. 7a) and $2^2\Pi \rightarrow 1^2\Pi$ (Fig. 7b). In the doublet manifold the rotational coupling may be the dominant one as illustrated in Fig. 7b. Indeed, the cross section of the $2^2\Pi \rightarrow 1^2\Sigma$ transition exceeds that of the $2^2\Pi \rightarrow 1^2\Sigma$ process.

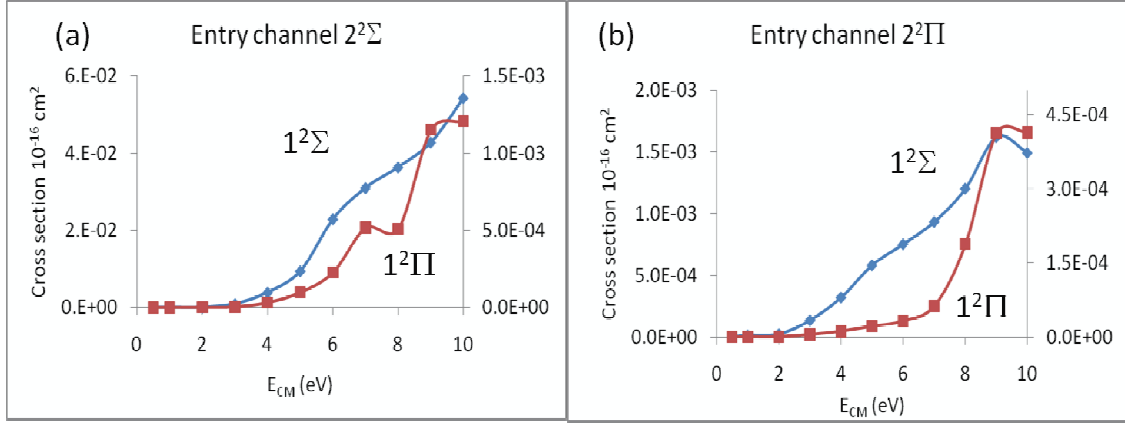


Fig. 7. Total cross section computed by Eq. (2-6) for a relative energy E_{CM} in the range 0.5 to 10 eV. Panel (a): entrance channel $2^2\Sigma$ $\{C(2s^22p^2)^3P + S^+(3s^23p^3)^2D\}$, panel (b): entrance channel $2^2\Pi$ $\{C(2s^22p^2)^3P + S^+(3s^23p^3)^2D\}$. Primary axis: exit channel $1^2\Sigma$ $\{C^+(2s^22p)^2P + S(3s^23p^4)^1D\}$, secondary axis: exit channel $1^2\Pi$ $\{C^+(2s^22p)^2P + S(3s^23p^4)^1D\}$.

As discussed in the following sections, the total charge transfer cross section taking into account the statistical weights is dominated by the quartet manifold (see Figs. 10 and 11). Some characteristics can be pointed out. For a given initial E_{CM} in an entry channel, the partial cross section involving Σ states is always larger for the quartets than for the doublets. This can be related to the different shapes of the potential energy curves (see Fig. 1) leading to very different kinetic energy at the crossing points and thus to different transition probabilities even if the radial couplings are quite similar. In the quartet manifold, the cross sections driven by radial couplings follow the order: $\sigma(2^4\Pi \rightarrow 3^4\Pi) > \sigma(2^4\Sigma \rightarrow 1^4\Sigma) > \sigma(2^4\Pi \rightarrow 1^4\Pi)$. The magnitude of the first two ones is in agreement with the strength of the interaction (see Fig.2b) and the smallness of the third one is due to the quasi completely diabatic behaviour at each passage at the peaked coupling at $R = 2.7$ u.a.. All the cross sections of the quartets due to rotational couplings have the same order of magnitude and are smaller than the sections involving radial couplings.

3. 3. Semi-classical cross section

In order to compare with quantum wave packet cross sections, the collision dynamics has been performed for the direct reaction $C^+(2s^22p)^2P + S(3s^23p^4)^3P \rightarrow C(2s^22p^2)^3P + S^+(3s^23p^3)^4S$ for a wide range of collision velocities from keV to eV collision energies. At such low velocities, the approximation of a straight-line trajectory for the nucleus motion may

be questionable and trajectory effects should be considered. Effectively, the approximation of a classical motion for the nucleus requires that the wavelength λ associated to the nuclear motion remains small compared with the size of the interacting region. In terms of the incident velocity v , this could be achieved if $\lambda = 2\pi/\mu v$ remains small over a distance about $a_0 = 1 \text{ a.u.}$ [28] and semiclassical approaches may be considered as valid down to incident energies of a few eV/amu [5], corresponding to velocities down to 0.02 a.u. ($E_{\text{CM}} \approx 80 \text{ eV}$) or a bit lower. In our calculation, the method has been extended to its limit and results at very low collision energies have to be considered as qualitative.

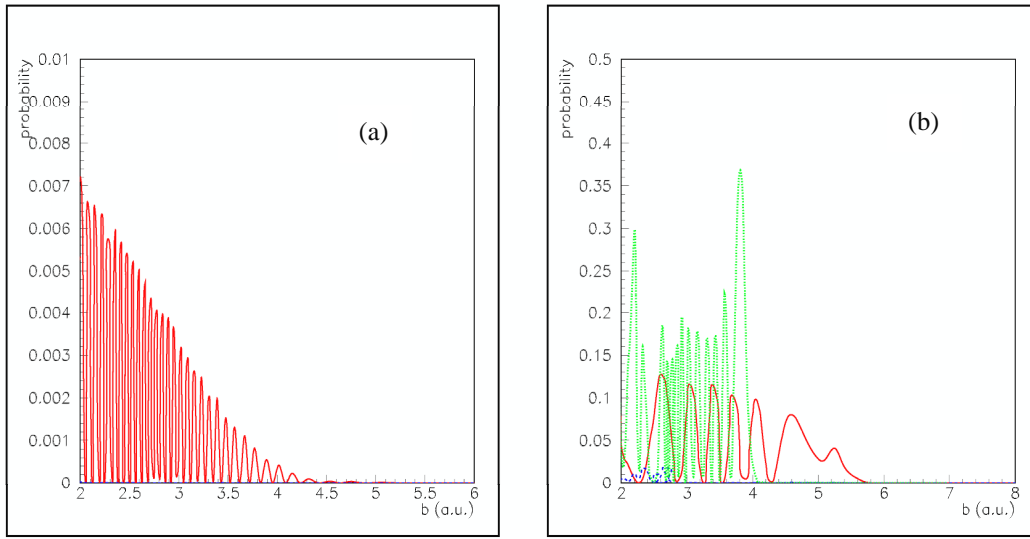


Fig. 8. Transition probabilities of occupying the exit channel $1\{C(2s^22p^2)^3P + S^+(3s^23p^3)^4S\}$ when the entrance channel is $2\{C^+(2s^22p)^2P + S(3s^23p^4)^3P\}$ as a function of the impact parameter b for a collision velocity $v=0.00677 \text{ a.u.}$ ($E_{\text{cm}}=10 \text{ eV}$). Panel (a): doublet manifold; red-full line, $2^2\Sigma \rightarrow 1^2\Sigma$; blue-dashed line, $2^2\Pi \rightarrow 1^2\Pi$. Panel (b): quartet manifold; red-full line, $2^4\Sigma \rightarrow 1^4\Sigma$; blue-dashed line, $2^4\Pi \rightarrow 1^4\Pi$; green-dotted line, $2^4\Pi \rightarrow 3^4\Pi\{C(2s^22p^2)^1D + S^+(3s^23p^3)^4S\}$.

The transition probabilities with regard to the impact parameter b are presented in Fig. 8a,b for the doublet and quartet manifolds respectively for a relative collision energy $E_{\text{cm}} = 10 \text{ eV}$. The transition probabilities between entry and exit $^2\Sigma$ channels decrease rapidly with b . They remain small for all impact parameters, in agreement with the smooth avoided crossing between both states. The corresponding probability between $^2\Pi$ channels is almost zero all over the impact parameter range showing the diabatic behaviour of the short range avoided

crossing. The behaviour of the transition probabilities for quartet states appears quite different. The probabilities remain around 0.1 a.u. for the $2^4\Sigma\{C^+(2s^22p)^2P + S(3s^23p^4)^3P\} \rightarrow 1^4\Sigma\{C(2s^22p^2)^3P + S^+(3s^23p^3)^4S\}$ charge transfer for impact parameters up to $b \approx 6$ a.u.. However, the most important transition probability appears between the $2^4\Pi\{C^+(2s^22p)^2P + S(3s^23p^4)^3P\}$ and $3^4\Pi\{C(2s^22p^2)^1D + S^+(3s^23p^3)^4S\}$ channels. It may be relied directly to the strong avoided crossing between these states and show the importance of the excited $C(^1D) + S(^4S)$ exit channel in the quartet manifold. The corresponding transition probability is enhanced up to 0.37 a.u. for impact parameters around 4 a.u. On the contrary, the transition probability between $2^4\Pi$ and $1^4\Pi$ remains small as already noticed for the $2^2\Pi$ states. As pointed out in previous paragraph, the sharp peaks presented by the radial coupling matrix elements between $2,4\Pi$ states, radp12 , at short range appear as quasi-diabatic in the collision dynamics. This is the case for the $2^2\Pi$ states, but also for the 4Π levels which present however an extremely sharp radial coupling radp12 .

These semi-classical transition probabilities may be compared to the corresponding probabilities extracted from the quantal wave packet approach. The results are presented in

Fig. 9a,b where the $|S_{if}|^2$ elements are drawn as a function of $b = \sqrt{K(K+1)\hbar} / \mu v$

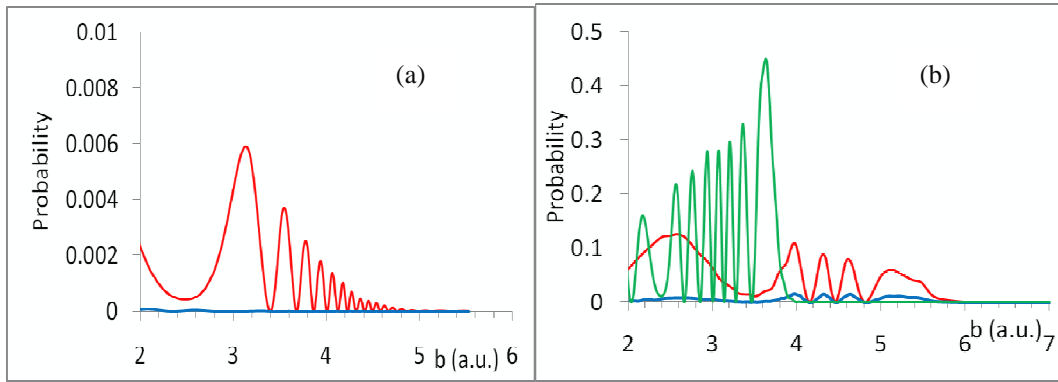


Fig. 9. $|S_{if}|^2$ matrix elements drawn as a function of the classical impact parameter b for the exit channel $1\{C(2s^22p^2)^3P + S^+(3s^23p^3)^4S\}$ when the entrance channel is $2\{C^+(2s^22p)^2P + S(3s^23p^4)^3P\}$ for a collision relative kinetic energy $E_{\text{cm}}=10$ eV. Panel (a): doublet manifold; red-full line, $2^2\Sigma \rightarrow 1^2\Sigma$; blue-dashed line, $2^2\Pi \rightarrow 1^2\Pi$. Panel (b): quartet manifold; red-full line, $2^4\Sigma \rightarrow 1^4\Sigma$; blue-dashed line, $2^4\Pi \rightarrow 1^4\Pi$; green-dotted line, $2^4\Pi \rightarrow 3^4\Pi\{C(2s^22p^2)^1D + S^+(3s^23p^3)^4S\}$.

The general behaviour is quite the same in both calculations, showing a rapid decrease with increasing impact parameter for the probability between the entry and exit $2^2\Sigma$ channels. The

transition probabilities reach about 0.006 a.u. at the maximum and are almost zero for impact parameters above 5 a.u. ($K > 550$), in quite good agreement with the previous semi-classical results. As previously noticed, the probability between ${}^2\Pi$ channels is almost zero. The importance of the strong avoided crossing between ${}^2\Pi\{C^+(2s^22p)^2P + S(3s^23p^4)^3P\}$ and ${}^3\Pi\{C(2s^22p^2)^1D + S^+(3s^23p^3)^4S\}$ is also observable with a regular increase of the transition probability up to about 0.4 a.u. for impact parameter around 4. a.u. ($K \approx 390$) The corresponding transition probabilities for the ${}^2\Sigma\{C^+(2s^22p)^2P + S(3s^23p^4)^3P\} \rightarrow {}^1\Sigma\{C(2s^22p^2)^3P + S^+(3s^23p^3)^4S\}$ remain around 0.1 a.u. up to $b \approx 6$. a.u. ($K \approx 640$) as previously noticed on the semi-classical calculation and the transition probability between ${}^2\Pi$ and ${}^1\Pi$ remains very small, as already pointed out for the ${}^2\Pi$ states.

With consideration of statistical weights between Σ and Π states, the cross sections σ^Σ and σ^Π for Σ and Π states respectively

$${}^{2,4}\sigma = \frac{1}{3} \sigma^\Sigma + \frac{2}{3} \sigma^\Pi.$$

The total cross section taking account simultaneously of doublet and quartet channels may then be expressed by:

$$\sigma_{tot} = \frac{1}{3} {}^2\sigma + \frac{2}{3} {}^4\sigma.$$

taking account of the statistical weights between doublet and quartet manifolds.

The semi-classical partial and total cross sections are presented in Fig. 10. With regard to statistical weights, the quartet states provide the main contribution to the total cross section at low collision energies. As shown clearly from the transition probabilities, the consideration of the upper ${}^4\Pi\{C(2s^22p^2)^1D + S^+(3s^23p^3)^4S\}$ level is necessary for an accurate description of the system and the corresponding interaction is determinant for a correct determination of the partial cross section. The quartet cross sections remain above 10^{-16} cm^2 , even at low energies. On the contrary, the doublet cross sections decrease strongly at lower collision energies.

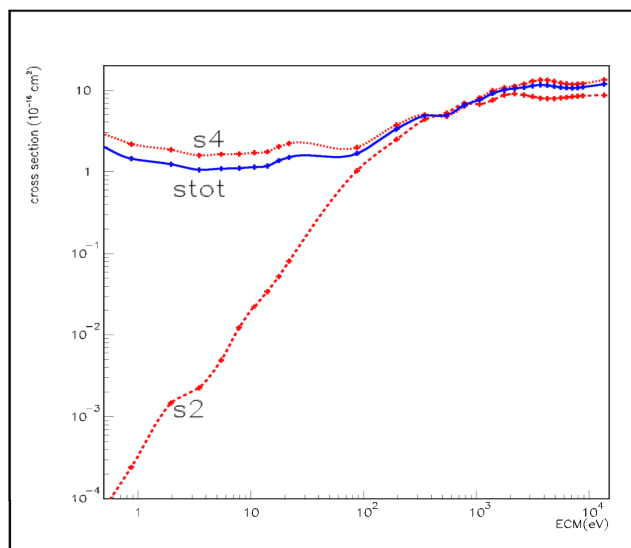


Fig. 10: Semiclassical partial (doublets: s2, quartets:s4) and total cross sections (stot) for the the CS^+ molecular system in the 0.5eV-10keV E_{CM} energy range: doublet manifold (dashed line); quartet manifold (dotted line); total cross section (solid line).

3. 4. Cross sections and rate constant

In order to analyze the validity of the semiclassical method at low energy, a comparison of the semiclassical and quantal wave packet dynamics approaches may be driven in the energy range where both calculations are available. The objective is also, for astrophysical interest, to extract precise cross sections in the low to medium energy domain in order to determine with the best accuracy possible the rate constants for the direct charge transfer process $\text{C}^+(2s^22p)^2\text{P} + \text{S}(3s^23p^4)^3\text{P} \rightarrow \text{C}(2s^22p^2)^3\text{P} + \text{S}^+(3s^23p^3)^4\text{P}$ and its reverse reaction.

The wave packet dynamics has been performed in the 0.5-20 eV centre-of-mass energy range, where the semiclassical method has been extended. A zoom of the cross sections in this energy domain is presented in Fig. 11.

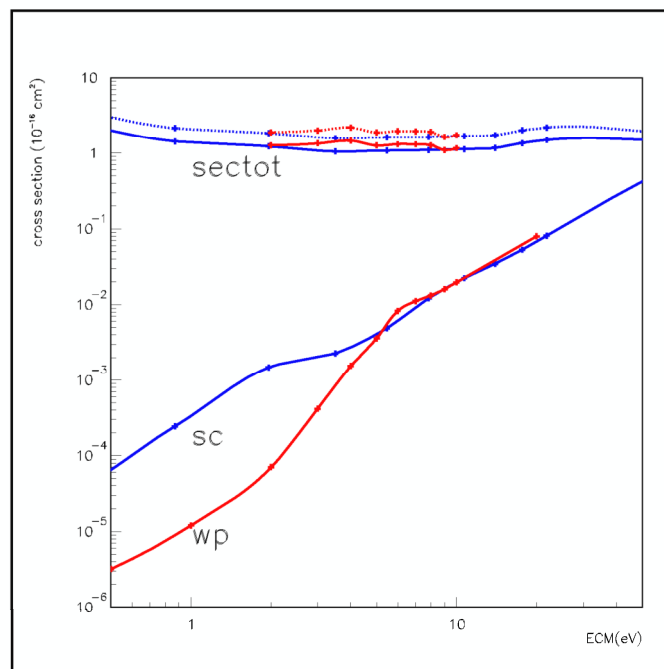


Fig. 11: Semiclassical (blue) and wave packet (red) partial and total cross sections for the CS^+ molecular system in the 0.5eV-50 eV E_{CM} energy range: doublet manifold (solid line); quartet manifold (dotted line); total cross section (solid line).

The semiclassical partial cross sections for the doublet manifold appear in excellent agreement with the quantal wave packet approach for collision energies higher than 8-10 eV. This is a very interesting result as it allows the use of such semiclassical approaches far below the generally accepted domain of accuracy. As expected, the quantal calculation deviates at lower energies from the semiclassical one. The variation is less sensitive for the quartet cross sections; the wave packet values remain always close to the previous semiclassical ones, even at energies down to 1eV. As the quartet manifold corresponds to a statistical weight two times higher than the doublet one, the total cross sections remain close in wave packet and semiclassical approaches, even at energies low with regard to the domain of validity of the semiclassical method. Such a result is very encouraging in order to have, at low price, an order of magnitude of cross sections, and consequently rate coefficients, for a number of astrophysical processes, in particular charge transfer processes, and validates our previous semiclassical treatment.

Anyway, in order to have the most precise evaluation for the present $C^+(2s^22p)^2P + S(3s^23p^4)^3P \rightarrow C(2s^22p^2)^3P + S^+(3s^23p^3)^4P$ charge transfer process, the calculation of rate constants has been performed using for doublet and quartet manifolds, the cross sections determined by means of the wave packet quantal approach in the 0.5-10eV collision range, completed by the semiclassical values at higher collision energies. The rate constants for the direct reaction $C^+(2s^22p)^2P + S(3s^23p^4)^3P \rightarrow C(2s^22p^2)^3P + S^+(3s^23p^3)^4S$ are presented in Table 2 and compared to a full semiclassical calculation.

Table 2. Rate coefficients for the $C^+ + S$ and reverse reaction (in cm^3s^{-1})

T(K)	$C^+(^2P) + S(^3P) \rightarrow C(^3P) + S^+(^4S)$		$C(^3P) + S^+(^4S) \rightarrow C^+(^2P) + S(^3P)$	
	Semiclassic	wave packet	semiclassic	wavepacket
500	1.8×10^{-11}	1.3×10^{-11}	–	–
1000	3.8×10^{-11}	3.7×10^{-11}	2.6×10^{-15}	2.5×10^{-15}
5000	7.3×10^{-11}	8.7×10^{-11}	2.6×10^{-11}	3.1×10^{-11}
10000	7.3×10^{-11}	1.0×10^{-10}	7.5×10^{-11}	1.3×10^{-10}
50000	1.3×10^{-10}	1.5×10^{-10}	3.1×10^{-10}	3.6×10^{-10}
100000	2.0×10^{-10}	2.2×10^{-10}	5.5×10^{-10}	5.9×10^{-10}

As expected from the cross section calculations, the difference between semiclassical and quantal wave packet rate coefficients is relatively weak. The relative error bar is about 10-20% for most of the temperatures with anyway a higher error of 37% at 10000K and an exceptionally good agreement at 1000K. Considering absolute values, rate constants for the direct process are small, about $8. \times 10^{-11} \text{ cm}^3\text{s}^{-1}$ at 5000K. Such a value is significantly lower than the suggested one $1.5 \times 10^{-9} \text{ cm}^3\text{s}^{-1}$ given in the UMIST data base [11] for the 10K-41000K temperature range. However, the variation of the calculated rate coefficients is relatively weak in a wide temperature domain and a value of about $1. \times 10^{-10} \text{ cm}^3\text{s}^{-1}$ may be assumed in the 5000-50000K temperature range with a reasonable accuracy. This result is in accordance with the constant value considered in astrophysical models; the usual value seems to be overestimated by about a power of 10.

The total rate constant for the reverse process $C(^3P) + S^+(^4S) \rightarrow C^+(2s^22p)^2P + S(3s^23p^4)^3P$ has been deduced from the symmetry properties of the S-matrix following equation (2-8). The degeneracy is $g = 3$ with regard to the multiplicity of initial and final states and the energy gain is $\Delta E = 0.92\text{eV}$. The rate constants are presented in Table 2. As noticed for the direct process, the relative error between semiclassical and wavepacket values are about 10-20% with anyway a maximum at 10000K. The rate constants increase significantly with temperature. They are about $3.\times 10^{-10} \text{ cm}^3\text{s}^{-1}$ at 5000K but become rapidly negligible for lower temperatures because of the exponential factor.

4. Concluding remarks

The $C^+(2s^22p)^2P + S(3s^23p^4)^3P$ charge transfer process and its reverse reaction have been studied by means of quantum dynamics wave packet methods and compared to semiclassical results. The present quantum approach provides a precise determination of cross sections in the low energy domain and shows an excellent correlation with the semiclassical calculations, valid at higher energies. These semiclassical values slightly differ from the previous results given in ref 12 since new radial non adiabatic couplings have been used in this work. However, the general behaviour remains the same and we confirm the dominant role of the quartet manifold in the charge transfer. Such a treatment gives access to precise values of the rate coefficients for the direct $C^+(2s^22p)^2P + S(3s^23p^4)^3P$ and reverse charge transfer processes. Furthermore, in this case, it validates the semiclassical approach in an extended energy domain which could be a useful tool for rate constant determination of such processes. The wave packet approach is indeed computational-time consuming and efficient only in a limited range of relative kinetic energy from 0.5 or 1eV to 20 eV. At very low energy, spreading and formation of shape resonances are unfavourable factors. At higher energy the number of partial waves K to ensure convergence of the cross section and thus the number of propagations become very large. The computational time also increases particularly when the process involves a lot of electronic states so that parallelization is advised. However, time dependent methods remain appealing to decipher some mechanisms, for instance the formation of metastable states in exit channels during the collisions as it has been illustrated here.

Acknowledgments

We thank J. M. Teuler for his help with computational issues. This work is granted access to

the HPC resources of CCRT/CINES/IDRIS under the allocations 2010-[i2010081655 and i2010081566] made by GENCI [Grand Equipement National de Calcul Intensif]. The financial support of the FNRS of Belgium in the University of Liège Nic3 project is gratefully acknowledged. We thank the support of the COST Action CM0702 CUSPFEL.

References

- ¹ Hayes M A, Nussbaumer H 1986, *Astrophys. J.* **161**, 287
- ² Sandlin G D, Bartoe J D F, Baureckner G F, Tousey R, Van Hoosier ME 1986 *Astrophys. J. Suppl.* **61**, 801
- ³ Nussbaumer H 1986 *Astron. Astrophys.* **155**, 205
- ⁴ Honvault P, Gargaud M, Bacchus-Montabonel M C, McCarroll R, 1995 *Astron. Astrophys.* **302**, 931
- ⁵ Gargaud M, Bacchus-Montabonel M C, McCarroll R 1993 *J. Chem. Phys.* **99**, 4495
- ⁶ Bacchus-Montabonel M C, Courbin C, McCarroll R 1991 *J. Phys. B* **24**, 4409
- ⁷ Bacchus-Montabonel M C 1999 *Phys. Rev. A* **59**, 3569
- ⁸ Baliunas S L and Butler S E 1980 *Astrophys. J.* **235**, L45
- ⁹ Le Bourlot J, Pineau des Forêts G, Roueff E, Flower D R, 1993 *Astron. Astrophys.* **267**, 233
- ¹⁰ Teyssier D, Fosse D, Gerin M, Pety J, Abergel A, Roueff E 2004 *Astron. Astrophys.* **417**, 135
- ¹¹ The *UMIST database for Astrochemistry* <http://www.udfa.net>.
- ¹² Bacchus-Montabonel M C and Talbi D 2008 *Chem. Phys. Lett.* **467**, 28
- ¹³ Zare R N *Angular Momentum*, 1988, World Scientific, New York
- ¹⁴ Shtermin P S and Vasyutinskii O S 2008 *J. Chem. Phys.* **128**, 194314
- ¹⁵ Vaeck N, Bacchus-Montabonel M C, Baloitcha E, Desouter-Lecomte M 2001 *Phys. Rev. A* **63**, 042704
- ¹⁶ Bacchus-Montabonel M C and Fraija F 1994 *Phys. Rev. A* **49**, 5108
- ¹⁷ Smith F T 1969 *Phys. Rev.* **179**, 111
- ¹⁸ Lefebvre-Brion H and Field R W *The Spectra and Dynamics of Diatomic Molecules* 2004 Elsevier Academic Press, Amsterdam
- ¹⁹ Werner H J, Knowles P J, MOLPRO (version 2009.1) package of ab-initio programs.
- ²⁰ Fraija F, Allouche A R, Bacchus-Montabonel M C 1994 *Phys. Rev. A* **49**, 272
- ²¹ Errea L F, Mendez L, Riera A 1982 *J. Phys. B.* **15**, 101
- ²² Zeng J and Zhang H, *Theory and Application of Quantum Molecular Dynamics*, 1999, World Scientific Publishing, Singapore
- ²³ Jäckle A and Meyer H-D 1996 *J. Chem. Phys.* **105**, 6779
- ²⁴ Baloitcha E, Desouter-Lecomte M, Bacchus-Montabonel M C and Vaeck N 2001 *J. Chem. Phys.* **114**, 8741
- ²⁵ Loreau J, Sodoga K, Lauvergnat D, Desouter-Lecomte M and Vaeck N 2010 *Phys. Rev. A* **82**, 012708
- ²⁶ Feit M D, Fleck J A and Steiger A 1982 *J. Comput. Phys.* **47**, 412
- ²⁷ Alvarillos J and Metiu H, 1988 *J. Chem. Phys.* **88**, 4957
- ²⁸ Bransden B H and McDowell M R C 1992 *Charge Exchange and the theory of Ion-Atom collisions*, Clarendon Press, Oxford
- ²⁹ Allan R J, Courbin C, Salas P and Wahnou P 1990 *J. Phys. B* **23**, L461
- ³⁰ Nicklass A, Dolg M, Stoll H, Preuss H 1995 *J. Chem. Phys.* **102**, 8942
- ³¹ Woon D E, Dunning T H Jr 1993 *J. Chem. Phys.* **98**, 1358

³² *NIST Atomic Spectra Database Levels* http://www.physics.nist.gov/cgi-bin/AtData/main_asd

³³ Larsson M 1985 *Chem. Phys. Lett.* **117**, 33

³⁴ Honjou N 2008 *Chem. Phys.* **344**, 128